Nanoscale Joule Heating and Electromigration Enhanced Ripening of Silver Nanowire Contacts

Tze-Bin Song,[†,‡] Yu Chen,[†,‡] Choong-Heui Chung,[†,‡,§] Yang (Michael) Yang,[†] Brion Bob,[†,‡] Hsin-Sheng Duan,[†,‡] Gang Li,[†] King-Ning Tu,[†,*] Yu Huang,[†,‡,*] and Yang Yang[†,‡,*]

[†]Department of Materials Science and Engineering and [‡]California NanoSystems Institute, University of California Los Angeles, Los Angeles, California 90095, United States and [§]Department of Materials Science and Engineering, Hanbat National University, Daejeon 305-719, Korea

ABSTRACT Solution-processed metallic nanowire thin film is a promising candidate to replace traditional indium tin oxide as the next-generation transparent and flexible electrode. To date however, the performance of these electrodes is limited by the high contact resistance between contacting nanowires; so improving the point contacts between these nanowires remains a major challenge. Existing methods for reducing the contact resistance require either a high processing power, long treatment time, or the addition of chemical reagents, which could lead to increased manufacturing cost and damage the underlying substrate or device. Here, a nanoscale point reaction process is introduced as a fast and low-power-consumption way to improve the electrical contact properties between metallic nanowires. This is achieved *via* current-assisted localized joule heating accompanied by electromigration. Localized joule heating effectively targets the high-resistance contact points between nanowires, leading to the automatic removal of surface ligands, welding of contacting nanowires, and the reshaping of the contact pathway between the nanowires to form a more desirable geometry of low resistance for interwire conduction. This result shows the interplay between thermal and electrical interactions at the highly reactive nanocontacts and highlights the control of the nanoscale reaction as a simple and effective way of turning individual metallic nanowires into a highly conductive interconnected nanowire network. The temperature of the adjacent device layers can be kept close to room temperature during the process, making this method especially suitable for use in devices containing thermally sensitive materials such as polymer solar cells.

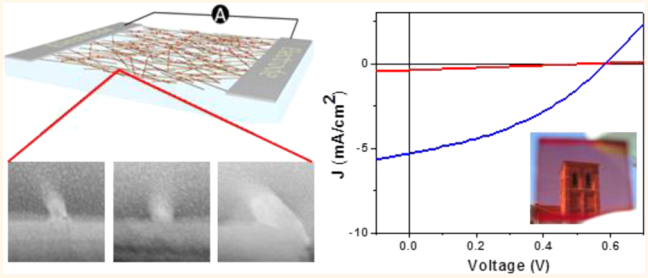

KEYWORDS: elecromigration · ripening · joule heating · transparent electrode · silver nanowire · solution process · polymer solar cell

The excellent mechanical, optical, electrical, and thermal properties of low-dimensional materials,[1−4] such as nanowires (NWs), nanoparticles (NPs), and nanotubes (NTs) have attracted people's attention and have been applied to a number of fields including optical electronics,[5] energy storage,[6] and sensors.[7] With the recent demand for thin, transparent, conducting films and flexible devices, nanomaterials such as carbon nanotubes,[8,9] graviaphene,[10,11] and metallic nanowires[12−14] have emerged as promising alternatives to replace the brittle indium tin oxide (ITO). In particular, silver nanowire (AgNW) networks provide excellent transmittance and conductance and thus have been brought forward as a potential candidate for transparent conductors (TCs) in thin film optoelectronic devices,[15] such as touch panels, light emitting diodes (LEDs), and solar cells, due to their potential high-throughput, low-cost fabrication, flexibility, and solution-processability. However, the high contact resistance between silver nanowires coming from the insulating surfactant coating of polyvinylpyrrolidone (PVP) and loose contact between individual AgNWs remains a critical issue, making extra processing steps necessary in order to achieve low sheet resistance values desirable for practical applications.[16]

Many processing techniques have been reported to address this issue, including heat treatment (featuring either a high processing temperature or long treatment time),[12] mechanical pressing,[17,18] electrochemical ion exchange,[19] vacuum filtration,[20] metal-oxide nanoparticle fusing,[21,22] and

* Address correspondence to kntu@ucla.edu (K.-N. Tu); yhuang@seas.ucla.edu (Y. Huang); yangy@ucla.edu (Y. Yang).

Received for review December 23, 2013 and accepted February 11, 2014.

Published online February 11, 2014
10.1021/nn4065567

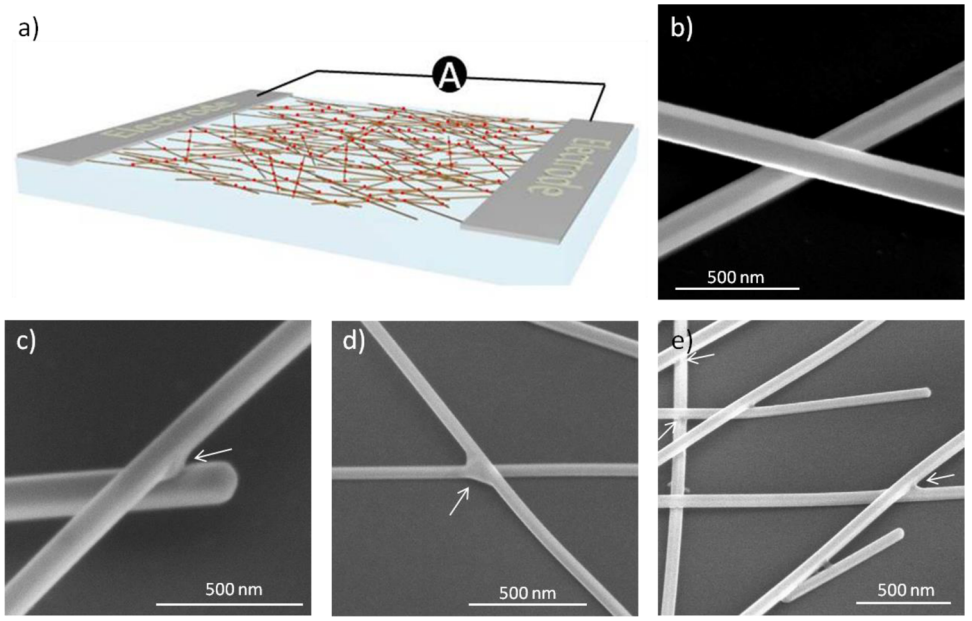

Figure 1. Experimental setup and scanning electron microscope (SEM) images before and after electrowelding treatment. (a) Schematic diagram of the experimental setup, with a continuous network of nanowires allowing for the passage of current between two metal electrodes. (b) Tilted (45°) SEM images of the initial silver nanowire contact. (c, d) Nanowire contacts after the electrowelding treatment; different morphologies of the silver nanowire contacts are observed under tilted SEM. (e) Wider view of several nanowire contacts after the passage of current. The arrows indicate the deformation of the nanowire contacts.

plasmonic welding process.[23] Some of these methods require the use of high input powers or long treatment durations, while others suffer from obvious scalability issues and shadow effect or may damage chemically sensitive substrates. Recent reports demonstrated that joule heating can weld platinum wires and carbon nanotubes by precisely controlling the contact geometry and current flow between the two wires.[24,25] With the forming of point contacts, hot spots can be generated at the contact point because of the high local current density. In this work, passing current through the small contact points between the wires with residual insulating surface ligands from the chemical synthesis process successfully generated enough power to weld all the contacts of the wires across the entire large-area devices. During this process, electromigration occurred at the high current density regions in the nanowire network[26] in and near the contact region, which plays a critical role in determining the electrical properties of the metallic nanowires network and therefore is crucial for the future applications of the metallic nanowires. This method is easily transferable to large-scale AgNW networks, where substantial improvement in the conductivity of these silver nanowire network electrodes can be achieved at low temperatures and by using only a small amount of input energy over the treatment duration of a few seconds. This process enables us to obtain low-resistance AgNW networks and employ them as electrodes in devices that require relatively gentle processing conditions, such as polymer solar cells, in which an efficiency enhancement of 20 times is demonstrated in this work.

RESULTS AND DISCUSSION

A schematic diagram of the experimental setup is shown in Figure 1a, with the red dots indicating hot spots for the electrowelding process. The AgNWs were either synthesized according to previous reports[19] or commercially available AgNWs. AgNWs were spun-cast on a glass substrate (1.5 × 1.2 cm^2) patterned with evaporated metal electrodes to form the nanowire network, and a direct current bias was applied between the electrodes to allow current to flow through the nanowire network. In our experiment, a current limit was put in place and adjusted to prevent high-current breakdown of the network. The AgNW networks were characterized by scanning electron microscopy (SEM), spectrophotometry, and current−voltage measurements before and after the electric current treatment.

SEM images of the AgNW contacts before the electrical current treatment are shown in Figure 1b, and the sharp interface between the two nanowires in contact is clearly visible. After a current treatment at 0.2 A limit with 25 V compliance voltage for 30 s, different morphologies of contacts were formed and characterized using the tilt-angle SEM (Figure 1c,d). In the case shown in Figure 1c, the contact was welded and the top wire had deformed toward the bottom wire. Figure 1d showed a contact in which only one side of the contact welded significantly, forming an asymmetric contact morphology, which is not seen in those welded contacts produced by other treatment methods such as heating and plasmonic welding, which invariably produce a symmetric contact shape at the wire−wire contact. A low-magnification tilted SEM image was also

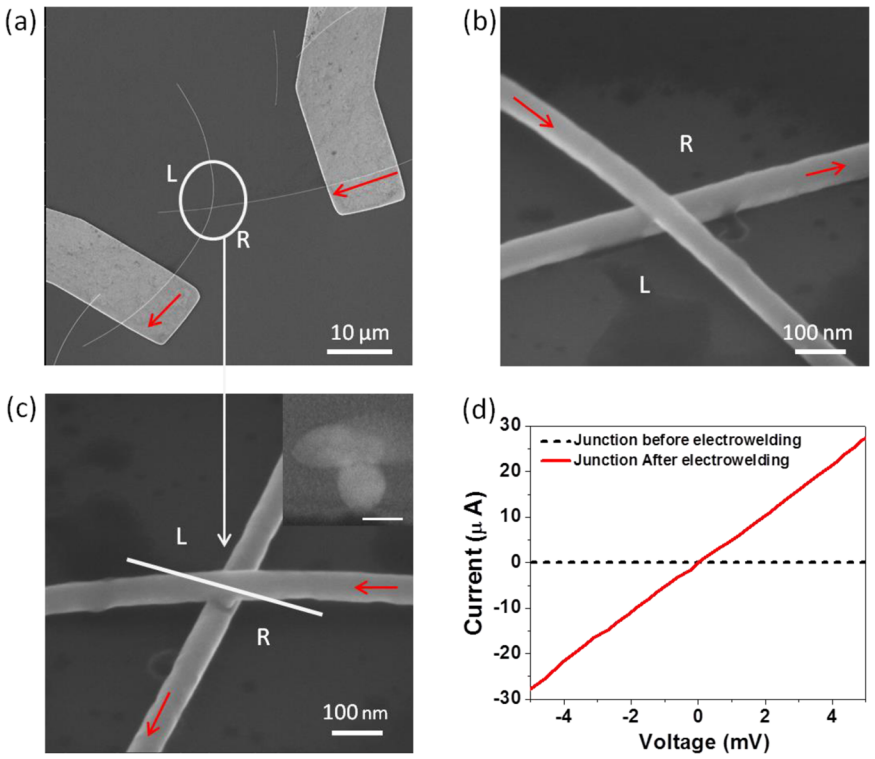

Figure 2. Two-wire contact measurement and characterization. (a) SEM image of a two-wire device, with the red arrows indicating the direction of current flow. (b, c) Tilted (52°) SEM image of the silver nanowire contact from the different directions. The diameters of the top nanowire and the bottom one are around 49 and 58 nm, respectively. The reacted contact was found at the R (right) corner of the silver nanowires. The cross-sectional SEM image of the two silver nanowires contact is shown in the inset of (c), with the majority of deformation clearly concentrated in the upper nanowire. The scale bar of the inset is 50 nm. (d) Current−voltage measurements before and after current passing. The current of the pristine device is in the pA region and the post-treatment device is in the μA, as shown.

taken after the treatment (Figure 1e), showing contact morphologies distinct from those produced by other processes.[23] The difference in the symmetry of the contact morphology indicates that a different joining mechanism is at work in our point contact treatment.

In order to further understand the reaction taking place at the contacts, an isolated two-wire contact system was fabricated, as shown in Figure 2a. The direction of the applied current is indicated by red arrows. A 500 ohm resistor was connected to introduce a current limit under 0.1 V bias for the structure. Before current treatment, the resistance of the two-wire device was larger than 10^{10} ohm due to the large point contact resistance. After the current treatment with a maximum current density of around 1.5×10^7 A/cm^2, calculated from the maximum current value to the cross section area of the small nanowire, the resistance was dramatically reduced to 185 ohm, as shown in the $I-V$ curves depicted in Figure 2d. The ratio between the power generated at the contact and within the nanowire can be expressed as $P_c/P_w = R_c/R_w$, in which R_c and R_w are the two-wire contact resistance and nanowire resistance, respectively. From experimental results, $R_c + R_w$ is larger than 10^{10} ohm, and we can estimate that the average R_w from AgNW dimensions should be around 180 ohm. This results in the conclusion $R_c \gg R_w$, indicating that nearly 100% of the heat generation will be localized at the contact with little heating effect in the bulk of the AgNWs. The contact morphology of the two-wire device was characterized from different viewing angles, left (L) and right (R), as shown in Figure 2a, after applying the electrical current (Figure 2b,c), and the same asymmetric shape of the contact similar to those in the larger film was observed. The cross-section of the contact was made using focused ion beam (FIB) and characterized with SEM to gain more insight into the contact formation. As shown in the inset of Figure 2c, the top nanowire deforms around the bottom nanowire, and the final contact shape formed to favor a good electrical connection between the two. It is observed that in general, the nanowire with the smaller diameter of the two tends to take on the majority of the morphological changes and the most extreme changes took place at the corner of the contact.

This process can be simulated using a finite-element method, showing three stages of reaction taking place corresponding to our previous observation from cross-sectional SEM images (Figure 3). The images in Figure 3 show only a quarter of the simulated structure to highlight the current distribution near the contact. In Figure 3a, the point contact between two pristine

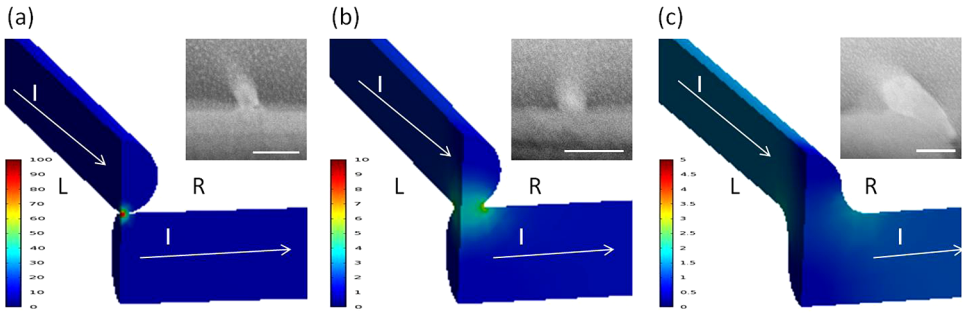

Figure 3. Finite-element simulation of the current density distribution at different contact morphologies. (a) Simulation and cross-sectional SEM of a pristine point contact between two silver nanowires. Extremely high current density occurs at the point contact. (b) Reacted contact morphology, showing the hot spot at the corner of the current flow direction. Localized high current densities can still occur under this morphology as larger amounts of current are forced through the contact. Electromigration can enhance the contact reaction and reshapes the contact into a ripened contact geometry. (c) Ripened contact morphology, producing greatly reduced current crowding and exhibiting a nearly uniform current density distribution through the contact. This morphology is more stable than the other two geometries and provides the best contact conductance due to its large contact area. The scale bars in each figure indicate the magnitude of the current density. The arrows indicate the current flow dirction. Insets in each simulated current density figures are FIB-cut cross-sectional SEM images of the different contact morphologies. The scale bar in each inset is 100 nm.

nanowires leads to current concentrating into a relatively small volume, and the presence of surfactants such as PVP will result in an even larger heat generation due to the high current density and high contact resistance. Under these conditions, strong joule heating will occur at the contact. Once enough heat is generated at the contact, increased surface and bulk diffusion of silver atoms will allow for the welding of the point contact to achieve a larger contact area. Furthermore, the tendency for the smaller nanowire to preferentially deform (as in Figure 1c) can be explained by the dependence of free energy on the diameter of the nanowire. According to Gibbs–Thomson theory, the Gibbs free energy increases sharply with smaller particle dimensions due to an increased contribution from the Gibbs–Thomson potential, $\Delta G = 2\gamma\Omega_m/r$, where γ is the surface energy, Ω_m is the volume per atom of investigated material, and r is the radius of the nanowires. The AgNW with the smaller diameter is subject to a higher potential energy and is therefore comparatively unstable compared to the larger wire. With the localized temperature increase produced by joule heating, the silver atoms in the smaller wire will obtain enough thermal energy to diffuse rapidly onto and around the other wire. Similar electrical sintering reactions in silver nanoparticles had been studied both experimentally and through simulation previously.[27−29] The reaction can happen on a time scale of milliseconds with a reaction temperature exceeding 100 °C.[27] It was established that the surface diffusion activation energy of noble metal atoms is typically less than 1 eV[30,31] and the process can happen even at room temperature. With the joule heating and the reduction of the surface diffusion activation energy from the high Gibbs–Thomson potential, the process can occur on a very short time scale. Eventually, a reacted contact is formed, generally adopting a shape similar to that shown in Figure 3b, which is reflected in the result in Figure 1c.

After the formation of the reacted contact, reduced contact resistance will allow for increased current flow. However, the current density will not be homogeneous across the entire contacted region because the contact area is still smaller than the bulk of the nanowires. Additionally, in order to minimize the distance electrons traveled as they travel from one nanowire to the other, current crowding occurred and the current density was substantially higher at the inner corner of the contact. As shown in Figure 3b, the highest current density region was at the corner of the contact instead of the center of the contact. This current crowding can introduce an enhancement to the local current density up to 1 order of magnitude from the simulation and previous report.[26] In a two-wire contact system, average current density was on the order of 10^7 A/cm^2, which indicated a current density of around 10^8 A/cm^2 at the corner of the contact. Comparing with the data from copper interconnect technology, surface diffusion induced electromigration occurs at the Si device operation temperature of 100 °C with a current density of 10^6 A/cm^2. The melting temperatures of silver and copper are similar; therefore the high current density induced by the current crowding in our two-wire contact system ensures that electromigration can occur. The high current density region will cause the formation of a hot spot at the corner of the contact between the two nanowires and facilitate continued atomic movement *via* sustained joule heating. Due to the fact that the directional current flow produces asymmetric heating (see Figure SI-1) on the L and R sides of the contact, the R corner of the reacted contacts will produce a stronger force driving atomic vacancies to the lower current density region from what is known as the collision effect, typical of current crowding situations. Eventually, the net motion of atoms toward the high current density region forms a ripened contact, with a typical geometry similar to

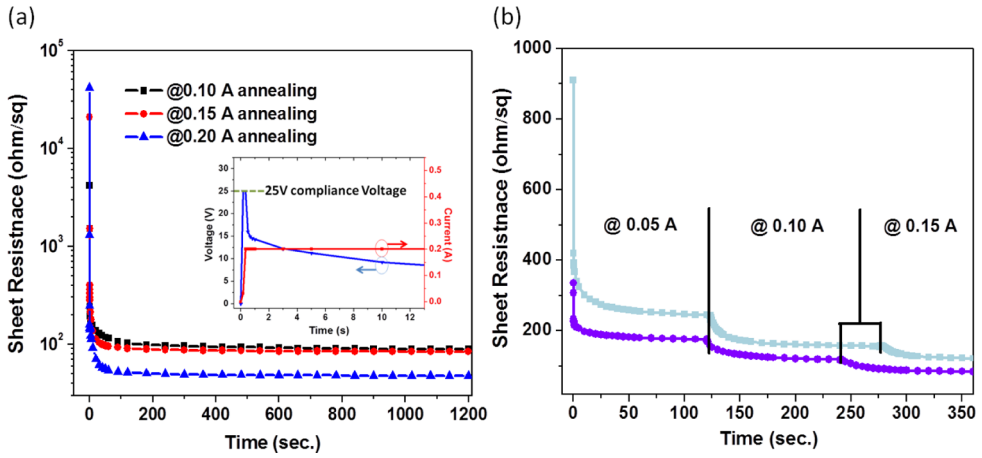

Figure 4. Controlling sheet resistance with time and current condition. (a) Sheet resistance changes with time under different constant current conditions. Different films were treated with 0.1, 0.15, and 0.2 amp and stabilized after around 30 s, with no significant changes after more than 20 min of continuous treatment. The voltage and current curves of 0.2 amp limit are shown in the inset. (b) Current limit controlled sheet resistance of two silver nanowire networks with different nanowire area densities. The current value was increased at the indicated times.

that shown in Figure 3c. The current density distribution in the ripened contact is more uniform than the previous two conditions (Figure 3a,b). Thus, the presence of the current crowding effects is likely the main reason behind the asymmetric shapes as those observed in the two-wire contact and nanowire network.

To demonstrate the feasibility and effectiveness of this process in device fabrication, the electrowelded AgNW network's performance as a transparent conductor is tested. The sheet resistance change as a function of treatment time was recorded under various current limits, as shown in Figure 4a. Three different densities of AgNW films were made with different initial sheet resistance values. The sheet resistance of all three films was significantly reduced by 1 to 3 orders of magnitude in the first 10 s of treatment, namely, 4×10^4 ohm/sq to 91 ohm/sq at 0.2 A current treatment and 4×10^3 ohm/sq to 157 ohm/sq at 0.1 A current treatment. After 30 s, the sheet resistance values saturated. Compared with those processed through thermal treatment on a hot plate, which requires temperatures of around 200 °C and treatment times of 10 to 20 min, this process is extremely fast and requires minimal power input into the nanowire network. Furthermore, this process can bring the sheet resistance down to a value comparable with reports from AgNW networks with the similar transmittance treated with a 200 °C heating process. In this case, the high initial contact resistance generated sufficient power at the contacts to enhance atomic diffusion and eventually induce current crowding effects to bring the contact resistance to a greatly reduced value similar to that observed in the two-wire contact system. Under constant current conditions, the required voltage from the power supply dropped dramatically as the contribution of contact resistance within the network diminished, and the power consumption dropped off sharply after the first seconds. The maximum power input to the network at the 0.2 A current treatment in Figure 4a was determined to be around 6.9 W/cm^2, and the total energy input of the entire treatment was roughly 94 J/cm^2 during the 30 s treatment period. The power consumption in this process is much lower than those reported for other treatment processes including pressure treatment and plasmonic welding, and its short processing time could make this process more suitable for mass production.[18,23] Additionally, when the current limit is increased to higher levels, the sheet resistance is further reduced, as shown in Figure 4b. The reduction in sheet resistance as the welding current is increased takes only a few seconds, similar to the duration of the initial process. The dependence of sheet resistance on welding current even after the initial treatment enables us to produce a continuously controllable resistance in AgNW networks, while opening up new avenues for the formation of well-controlled nanowire contact properties by electrical methods.

The optimized transmittance and sheet resistance (Figure 5a) values obtained from electrowelded nanowire networks were comparable to those calculated from the percolation theory[32−34] with a transmittance of 86.7% at 550 nm and a sheet resistance of 19.7 ohm/sq, indicating that this method is able to reduce the internanowire contact resistance in the nanowire networks to a negligible level.[34] To demonstrate the effectiveness of localized contact welding in practical applications, AgNW networks were incorporated into an organic photovoltaic (OPV) device as the top electrode. The AgNW network was spun-cast on top of fabricated polymer solar cell layers (ITO/ZnO/P3HT:PC_{60}BM/PEDOT:PSS) as the electrode, and the current density−voltage curve (J−V curve) was measured both before and after the electrowelding process. As shown

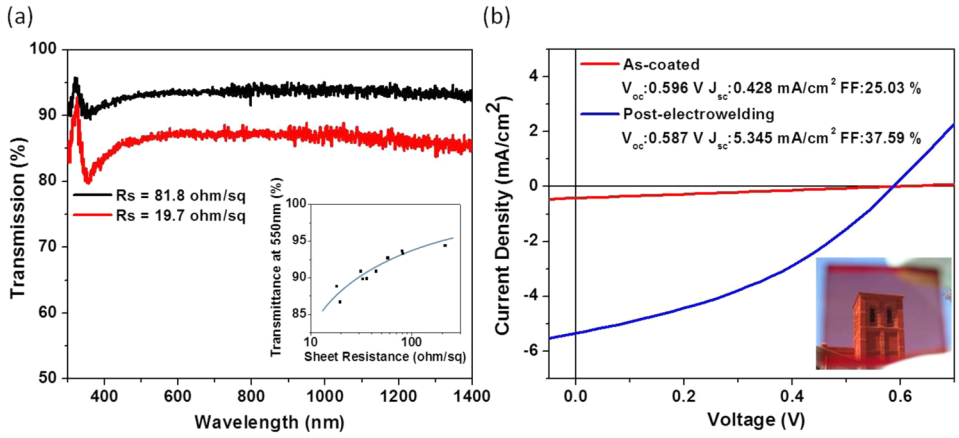

Figure 5. Optical properties and the application of electrowelding on temperature-sensitive materials and devices. (a) Transmission of treated silver nanowire films with different nanowire area densities. The inset shows the relationship between the transmission at 550 nm and electrowelded sheet resistance values with average nanowire dimensions of 90 nm in diameter and 40 μm in length. (b) Current density−voltage characterization of a semitransparent polymer solar cell made with an electrowelded silver nanowire film as the top electrode. The device using an untreated silver nanowire film (red curve) showed extremely high series resistance, and after the electrowelding treatment (blue curve) the series resistance was reduced significantly, indicating dramatically reduced sheet resistance in the silver nanowire film. The photovoltaic performance improves by a factor of 20 after the treatment. The inset is a picture of a semitransparent polymer solar cell.

in Figure 5b, the as-coated device shows an extremely low fill factor (FF) and short-circuit current density (J_{sc}). High internanowire contact resistance of the AgNW network appears to introduce a high series resistance into the device, which produced poor FF and J_{sc}. After the current treatment process, however, the FF and J_{sc} are significantly increased, with the FF increasing from 25.03% to 37.59% and J_{sc} from 0.428 mA/cm^2 to 5.345 mA/cm^2. From the $J-V$ curve, the series resistance was calculated to reduce from 1369 ohm/cm^2 to 7 ohm/cm^2. The power conversion efficiency was increased 20 times from 0.06% to 1.18% by the welding treatment. The lower sheet resistance of the AgNW network results in a more efficient transport of carriers and a reduction of the power loss within the AgNW electrode, which in turn leads to a higher fill factor, short-circuit current, and ultimately an enhanced solar cell efficiency. The fact that a stable V_{oc} value is attained after the treatment indicates that this current treatment process does not thermally damage the underneath layers, which can easily occur in relatively temperature sensitive OPV devices.

CONCLUSIONS AND PROSPECTS

We have demonstrated the use of localized reactions induced by electrical current flow to dramatically improve the contact properties of metallic nanowire contacts. This process can be precisely controlled using a constant current power supply to achieve different sheet resistance levels within seconds. Joule heating will initially be generated at the high-resistance contacts at the high current density region near the center of the wire/wire contact. The smaller diameter AgNW with a higher free energy will become unstable and diffuse onto the other wires to form reacted and eventually ripened contacts. Contact resistance was found to be reduced more than 7 orders of magnitude after the treatment. More importantly, the presence of an anisotropic electromigration effect was observed and resulted in further improvement of the morphology of the contact in bringing the contact resistance to lower values. This process demonstrated the capability of electrically controlling nanoscale interactions and introduced a new way to investigate nanowire contact reactions.

From a practical point of view, solution-based deposition and extremely fast post-treatments can facilitate the mass production of metallic nanowire networks. As demonstrated on polymer solar cells, power loss in the top electrode can be significantly reduced and the power conversion efficiency improved by 20 times after the treatment. Unlike heat treatment on a hot plate, this process makes it possible to develop a metallic nanowire as an electrode on temperature-sensitive substrates with low energy consumption and less damage. Additionally, this process will not suffer from shadowing effects, which can reduce process homogeneity over large areas in light or laser treatments. This development brings us one step closer to fast and cost-effective solution-processed electrodes, devices, and circuits fabricated on a wide variety of substrates through electrically derived contact reaction of nanomaterials and heterojunction nanostructure fabrication.

METHODS

Materials. AgNWs were obtained from Blue Nano Inc. (Charlotte, NC, USA). Poly(3-hexylthiophene) (P3HT) was purchased from Rieke Metals, Inc., and [6,6]-phenyl C61-butyric acid methyl ester ($PC_{60}BM$) was purchased from Nano-C (Westwood, MA, USA). Poly(3,4-ethylenedioxythiophene)/poly(styrenesulfonate)

(PEDOT:PSS, CLEVIOS P VP AI 4083) was purchased from H. C. Starck (Newton, MA, USA). ZnO nanoparticle solutions were prepared according to a previous report.[35]

Characterization of Silver Nanowire Electrodes. SEM images were taken on a Nova Nano 230 electron microscope, and cross-section SEM images were taken by a FEI Nova 600 Nanolab Dualbeam SEM/FIB for structural properties of the nanowire contact. The transmittance spectra were taken using a Hitachi ultraviolet−visible spectrophotometer (U-4100). Thermally evaporated Cr/Au (2 nm/50 nm) through the shadow mask was used as the metal pads on a glass substrate to define the 0.6 cm in length (L) and 1.2 cm in width (W) channel. The two-point probe method was used to estimate the sheet resistance of the film defined by $R_{sh} = R(W/L)$. After the annealing process, the sheet resistance was also tested using a four-point probe method with a sheet resistivity meter (Guardian Manufacturing, model SRM-232-100, range 0 to 100 ohm/sq) to varify the value. An HP E3631A Triple output direct current power supply with 25 V compliance voltage was used to apply current to the AgNW network. The resistance was converted by the voltage, and current recorded in the process and then transferred to the sheet resistance for comparison.

Device Fabrication and Characterization. Different AgNW area densities as transparent conductors are prepared by mulitple times of spin-casting with a AgNW dispersion. AgNWs are dispersed onto the SiO_2 substrate and then spin-coated with methyl methacrylate and poly(methyl methacrylate) as photoresists (PRs). In order to avoid thermal effects to the Ag wire contact, PRs are not baked after spin-coating. Ag films of 100 nm were patterned by e-beam lithography and then deposited to serve as electrodes. AgNW contact resistance measurements were performed on an Agilent semiconductor parameter analyzer using 0.1 V and connected to a 500 ohm resistor. The polymer solar cell device was fabricated on glass substrates with an ITO transparent electrode. The ZnO nanoparticles were dispersed in ethanol with a concentration of 0.1 wt %. The ZnO nanoparticle solution was spin-coated onto the substrate and then baked at 120 °C for 5 min under ambient conditions as the electron transport layer. P3HT:PC_{60}BM were blended (1:1, 2 wt % in dichlorobenzene) and spin-coated on the ZnO layer with the slow growth method.[36] After annealing at 110 °C for 10 min, the hole transporting material, PEDOT:PSS, was spin-coated on top of the active layer. Finally, AgNWs were spun-cast on top of PEDOT:PSS as the top electrode. $J-V$ characteristics of photovoltaic cells were taken using a Keithley 2400 source unit under a simulated AM1.5G spectrum with an Oriel 91191 solar simulator. The power was adjusted to 1 sun by comparing the current to a reference silicon photodiode, using a KG-5 filter to account for the spectral mismatch.

Simulation. Finite-element method simulations were performed using ANSYS Multiphysics software to demonstrate the current crowding at the nanowire contact points. The result showing full wires is shown in the Figure SI-1. Contacts with different morphologies were built based on the observation of SEM images by Solidwork software. The cross-section images were used to show the current ditribution in the bulk of the nanowires.

Conflict of Interest: The authors declare no competing financial interest.

Acknowledgment. The authors would like to express their gratitude for the generous financial support of Tokyo Electron Ltd. The authors thank Mr. Noah Bodzin from UCLA for assistant and discussion on SEM-FIB analysis.

Supporting Information Available: Current distribution by finite-element simulation in the full wires and cross-section mode on pristine, reacted, and ripened contact conditions. This material is available free of charge *via* the Internet at http://pubs.acs.org.

REFERENCES AND NOTES

1. Jing, G. Y.; Duan, H. L.; Sun, X. M.; Zhang, Z. S.; Xu, J.; Li, Y. D.; Wang, J. X.; Yu, D. P. Surface Effects on Elastic Properties of Silver Nanowires: Contact Atomic-Force Microscopy. *Phys. Rev. B* **2006**, *73*, 235409.
2. Cui, Y.; Lieber, C. M. Functional Nanoscale Electronic Devices Assembled Using Silicon Nanowire Building Blocks. *Science* **2001**, *291*, 851–853.
3. Balandin, A. A.; Ghosh, S.; Bao, W.; Calizo, I.; Teweldebrhan, D.; Miao, F.; Lau, C. N. Superior Thermal Conductivity of Single-Layer Graphene. *Nano Lett.* **2008**, *8*, 902–907.
4. Tao, A.; Sinsermsuksakul, P.; Yang, P. Tunable Plasmonic Lattices of Silver Nanocrystals. *Nat. Nanotechnol.* **2007**, *2*, 435–440.
5. Duan, X.; Huang, Y.; Cui, Y.; Wang, J.; Lieber, C. M. Indium Phosphide Nanowires as Building Blocks for Nanoscale Electronic and Optoelectronic Devices. *Nature* **2001**, *409*, 66–69.
6. Landi, B. J.; Ganter, M. J.; Cress, C. D.; DiLeo, R. A.; Raffaelle, R. P. Carbon Nanotubes for Lithium Ion Batteries. *Energy Environ. Sci.* **2009**, *2*, 638–654.
7. Kong, J.; Franklin, N. R.; Zhou, C.; Chapline, M. G.; Peng, S.; Cho, K.; Dai, H. Nanotube Molecular Wires as Chemical Sensors. *Science* **2000**, *287*, 622–625.
8. Wu, Z.; Chen, Z.; Du, X.; Logan, J. M.; Sippel, J.; Nikolou, M.; Kamaras, K.; Reynolds, J. R.; Tanner, D. B.; Hebard, A. F.; *et al.* Transparent, Conductive Carbon Nanotube Films. *Science* **2004**, *305*, 1273–1276.
9. Hu, L.; Hecht, D. S.; Gruner, G. Percolation in Transparent and Conducting Carbon Nanotube Networks. *Nano Lett.* **2004**, *4*, 2513–2517.
10. Khrapach, I.; Withers, F.; Bointon, T. H.; Polyushkin, D. K.; Barnes, W. L.; Russo, S.; Cracium, M. F. Novel Highly Conductive and Transparent Graphene-Based Conductors. *Adv. Mater.* **2012**, *24*, 2844–2849.
11. Bae, S.; Kim, H.; Lee, Y.; Xu, X.; Park, J. S.; Zheng, Y.; Balakrishnan, J.; Lei, T.; Kim, H. R.; Song, Y.; *et al.* Roll-to-Roll Production of 30-Inch Graphene Films for Transparent Electrodes. *Nat. Nanotechnol.* **2010**, *5*, 574–578.
12. Lee, J. Y.; Connor, S. T.; Cui, Y.; Peumans, P. Solution-Processed Metal Nanowire Mesh Transparent Electrodes. *Nano Lett.* **2008**, *8*, 689–692.
13. Chung, C. H.; Song, T. B.; Bob, B.; Duan, H. S.; Yang, Y. Silver Nanowire Composite Window Layers for Fully Solution-Deposited Thin-Film Photovoltaic Devices. *Adv. Mater.* **2012**, *24*, 5499–5504.
14. Rathmell, A. R.; Wiley, B. J. The Synthesis and Coating of Long, Thin Copper Nanowires to Make Flexible, Transparent Conducting Films on Plastic Substrates. *Adv. Mater.* **2011**, *23*, 4798–4803.
15. Barnes, T. M.; Reese, M. O.; Bergeson, J. D.; Larsen, B. A.; Blackburn, J. L.; Beard, M. C.; Bult, J.; Lagemaat, J. V. D. Comparing the Fundamental Physics and Device Performance of Transparent, Conductive Nanostructured Networks with Conventional Transparent Conducting Oxides. *Adv. Energy Mater.* **2012**, *2*, 353–360.
16. Hecht, D. S.; Hu, L.; Irvin, G. Emerging Transparent Electrodes Based on Thin Films of Carbon Nanotubes, Graphene, and Metallic Nanostructures. *Adv. Mater.* **2011**, *23*, 1482–1513.
17. Gaynor, W.; Lee, J. Y.; Peumans, P. Fully Solution-Processed Inverted Polymer Solar Cells with Laminated Nanowire Electrodes. *ACS Nano* **2010**, *4*, 30–34.
18. Tokuno, T.; Nogi, M.; Karakawa, M.; Jiu, J.; Nge, T. T.; Aso, Y.; Suganuma, K. Fabrication of Silver Nanowire Transparent Electrodes at Room Temperature. *Nano Res.* **2011**, *4*, 1215–1222.
19. Hu, L.; Kim, H. S.; Lee, J. Y.; Peumans, P.; Cui, Y. Scalable Coating and Properties of Transparent, Flexible, Silver Nanowire Electrodes. *ACS Nano* **2010**, *4*, 2955–2963.
20. Madaria, A. R.; Kumar, A.; Ishikawa, F. N.; Zhou, C. W. Uniform, Highly Conductive, and Patterned Transparent Films of a Percolating Silver Nanowire Network on Rigid and Flexible Substrates Using a Dry Transfer Technique. *Nano Res.* **2010**, *3*, 564–573.
21. Chung, C. H.; Song, T. B.; Bob, B.; Zhu, R.; Yang, Y. Solution-Processed Flexible Transparent Conductors Composed of Silver Nanowire Networks Embedded in Indium Tin Oxide Nanoparticle Matrices. *Nano Res.* **2012**, *5*, 805–814.

22. Zhu, R.; Chung, C. H.; Cha, K. C.; Yang, W.; Zheng, Y. B.; Zhou, H.; Song, T. B.; Chen, C. C.; Weiss, P. S.; Li, G.; *et al*. Fused Silver Nanowires with Metal Oxide Nanoparticles and Organic Polymers for Highly Transparent Conductors. *ACS Nano* **2011**, *5*, 9877–9882.
23. Garnett, E. C.; Cai, W.; Cha, J. J.; Mahmood, F.; Connor, S. T.; Christoforo, M. G.; Cui, Y.; McGehee, M. D.; Brongersma, M. L. Self-Limited Plasmonic Welding of Silver Nanowire Junctions. *Nat. Mater.* **2012**, *11*, 241–249.
24. Tohmyoh, H.; Fukui, S. Self-Completed Joule Heat Welding of Ultrathin Pt Wires. *Phys. Rev. B* **2009**, *80*, 155403.
25. Jin, C.; Suenaga, K.; Iijima, S. Plumbing Carbon Nanotubes. *Nat. Nanotechnol.* **2008**, *3*, 17–21.
26. Tu, K. N. Recent Advances on Electromigration in Very-Large-Scale-Integration of Interconnects. *J. Appl. Phys.* **2003**, *94*, 5451.
27. Allen, M. L.; Aronniemi, M.; Mattila, T.; Alastalo, A.; Ojanpera, K.; Suhonen, M.; Seppa, H. Electrical Sintering of Nanoparticle Structures. *Nanotechnology* **2008**, *19*, 175201.
28. Alastalo, A. T.; Seppa, H.; Leppäniemi, J. H.; Aronniemi, M. J.; Allen, M. L.; Mattila, T. Modeling of Nanoparticle Sintering under Electrical Boundary Conditions. *J. Phys. D: Appl. Phys.* **2010**, *43*, 485501.
29. Wakuda, D.; Kim, K. S.; Suganuma, K. Room-Temperature Sintering Process of Ag Nanoparticle Paste. *IEEE Trans. Compon. Packag. Technol.* **2009**, *32*, 627–632.
30. Iwama, S.; Hayakawa, K. Sintering of Ultrafine Metal Powders, II: Neck Growth Stage of Au, Ag, Al and Cu. *Jpn. J. Appl. Phys.* **1981**, *20*, 335–340.
31. Sanders, D. E.; DePristo, A. E. Predicted Diffusion Rates on FCC (001) Metal Surfaces for Adsorbate/Substrate Combinations of Ni, Cu, Rh, Pd, Ag, Pt, Au. *Surf. Sci.* **1992**, *260*, 116–128.
32. Bergin, S. M.; Chen, Y .H.; Rathmell, A. R.; Charbonneau, P.; Li, Z. Y.; Wiley, B. J. The Effect of Nanowire Length and Diameter on the Properties of Transparent, Conducting Nanowire Films. *Nanoscale* **2012**, *4*, 1996–2004.
33. Yu, Z.; Li, L.; Zhang, Q.; Hu, W.; Pei, Q. Silver Nanowire-Polymer Composite Electrodes for Efficient Polymer Solar Cells. *Adv. Mater.* **2011**, *23*, 4453–4457.
34. Sorel, S.; Lyons, P. E.; De, S.; Dickerson, J. C.; Coleman, J. N. The Dependence of the Optoelectrical Properties of Silver Nanowire Networks on Nanowire Length and Diameter. *Nanotechnology* **2012**, *23*, 185201.
35. Chou, C. H.; Kwan, W. L.; Hong, Z.; Chen, L. M.; Yang, Y. Metal-Oxide Interconnection Layer for Polymer Tandem Solar Cells with an Inverted Architecture. *Adv. Mater.* **2011**, *23*, 1282–1286.
36. Li, G.; Shrotriya, V.; Huang, J.; Yao, Y.; Moriarty, T.; Emery, K.; Yang, Y. High-Efficiency Solution Processable Polymer Photovoltaic Cells by Self-Organization of Polymer Blends. *Nat. Mater.* **2005**, *4*, 864–868.